

# Finite Element Simulation of Love Wave based SAW Delay Line using COMSOL Multiphysics

Shyam Trivedi<sup>1</sup>, Harshal B. Nemade<sup>2,\*</sup>

<sup>1</sup>Center for Nanotechnology, Indian Institute of Technology Guwahati,

<sup>2</sup>Department of Electronics and Electrical Engineering, Indian Institute of Technology Guwahati, India.

\*Corresponding author: [harshal@iitg.ernet.in](mailto:harshal@iitg.ernet.in)

**Abstract:** The paper presents 3D finite element simulation of Love wave based SAW delay line using COMSOL Multiphysics. The device consists of a  $36^\circ$ -YX Lithium Tantalate substrate covered with  $4.7 \mu\text{m}$  thick  $\text{SiO}_2$  waveguide layer operating at  $\lambda = 12 \mu\text{m}$ . The time response study is used to calculate the output voltages and normalized displacements in the device. The shear-horizontal wave nature of Love wave is confirmed from the result that in-plane shear horizontal displacements are much larger compared to vertical displacements. Impulse response is used to compute the insertion loss of the delay line. Thin PMMA layer is used to simulate mass loading on the device. The Love wave device offers a phase mass sensitivity of  $83.22 \text{ m}^2/\text{kg}$  which is consistent with previously reported values.

**Keywords:** Delay line, insertion loss, love wave mass sensitivity, SAW.

## 1. Introduction

A Surface acoustic wave (SAW) device generally consists of metal interdigital transducers (IDTs) made over a piezoelectric substrate. A SAW delay line device typically consists of input and output IDTs separated by a distance with absorbers at the ends to avoid reflections from the edges as shown in Fig. 1(a). Application of sinusoidal voltage to the input IDT launches an elastic wave on the surface of the substrate due to inverse piezoelectric effect [1]. The wave travels through the delay path and is received by the output IDT. The SAW delay line can be used as a sensor when sensing medium is present in the delay path as shown in Fig 1(b). The wave undergoes perturbation in velocity as it passes through the sensing region which gets detected in the form of phase change at the output IDT [2]. SAW delay line devices have been used in telecommunications industry

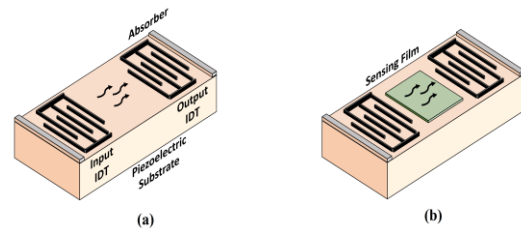


**Figure 1.** (a) Delay line (b) SAW delay line as sensor.

in designing high frequency filters [3] but they also find use in devising chemical, biological and gas sensors [4].

In the case of chemical or biological sensors mass loading is caused by the accumulation of target molecules in the chemical interface layer which is deposited on the sensing surface. This leads to change in velocity of the surface wave. Traditionally the change in mass loading is measured by using bulk acoustic wave (BAW) devices like quartz resonators consisting of thin quartz plates which are excited by electrodes on both sides of the quartz [5] but these devices suffer from low frequency of operation and low mass sensitivity. Rayleigh wave devices are SAW devices which provide large mass sensitivity and are excellent choice for designing gas sensors. However, when sensing in liquids, Rayleigh waves excite compressional waves in the adjacent liquid due to their particle displacement normal to the sensing surface, which leads to considerable acoustic losses making them unsuitable for liquid sensing applications [6].

A Love Wave (LW) device consists of a substrate that generates leaky SAW such as  $36^\circ$ -YX Lithium Tantalate (LT) or  $41^\circ$ -YX Lithium Niobate (LN), with a waveguiding layer present over it. The guiding layer helps to confine the wave energy at the surface which increases the mass sensitivity and coupling coefficient of the device [7]. In general, the LW device is advantageous over other type of devices in terms of high frequency of operation,

shielding metal IDTs from liquid, less attenuation in liquid due to shear horizontal nature of the wave and providing high mass sensitivity [8].

### 3. Simulation Methodology

The 3D geometry used for COMSOL simulation is shown in Fig. 2. Since piezoelectric crystals are anisotropic, a proper crystal cut and wave propagation direction is essential for simulation. We used the *rotated coordinate system* in order to rotate the Y-cut LiTaO<sub>3</sub> crystal by 36° with respect to the *x* axis to get the desired orientation of 36°-YX Lithium Tantalate. The device operates at  $\lambda = 12 \mu\text{m}$ . The input and output IDTs of Aluminum metal with electrode width  $\lambda/4$  are made over the substrate. We consider massless IDT electrodes to avoid the mass loading effect on the substrate, hence the thickness of IDT fingers is taken as zero.

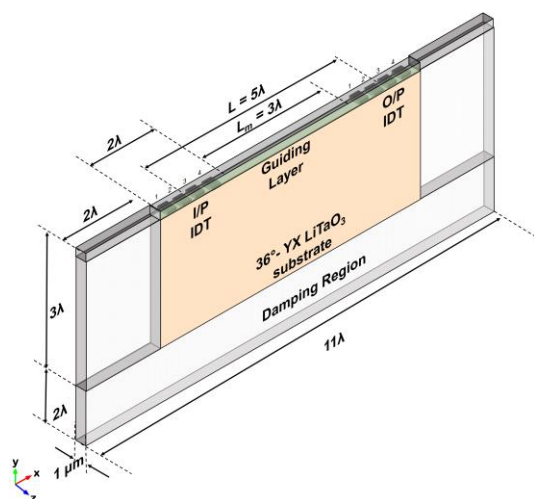


**Figure 2.** Simulation geometry of the Love wave based SAW delay line.

The IDT center to center distance ( $L$ ) is  $5\lambda$ . A mass loading region ( $L_m$ ) of  $3\lambda$  exists between the input and output IDT. The distance ( $D$ ) between the rightmost edge of input IDT and leftmost edge of output IDT is  $39 \mu\text{m}$ . A  $4.7 \mu\text{m}$  thick SiO<sub>2</sub> film is considered as waveguiding layer. To keep the simulation geometry small, *periodic boundary condition with continuity* is assumed along *z* axis which effectively make the IDTs of infinite aperture. It is represented as [9]

$$\Gamma_f(\mathbf{u}, V) = \Gamma_b(\mathbf{u}, V) \exp(-j2\pi\gamma n) \quad (1)$$

where  $\Gamma_f$  and  $\Gamma_b$  are the front and back portions of the simulation geometry in the *x-y* plane. Here,  $\mathbf{u}$  denotes the SAW displacement vector,  $\gamma$  is the complex propagation constant and  $V$  is the potential. The total displacement of the SAW is given by  $\sqrt{u_x^2 + u_y^2 + u_z^2}$  where  $u_x$ ,  $u_y$  and  $u_z$  are the particle displacements in *x*, *y* and *z* directions respectively. A critically damped region of size  $2\lambda$  is made to left of the input IDT, right of the output IDT and below the substrate so that there are no reflections from the edges of the device. The damping ratio is given as [10]

$$\xi_r = \frac{A_{dm} + B_{dk}\omega^2}{2\omega} \quad (2)$$

where  $\omega$  is the radian frequency of operation,  $A_{dm}$  and  $B_{dk}$  are the mass and stiffness proportional damping coefficients. The critical damping ( $\xi_r = 1$ ) can be achieved by keeping  $A_{dm} = 0$  and  $B_{dk} = 1/\pi f$ , where  $f = 325 \text{ MHz}$  is the frequency of operation. The second and fourth electrode of input IDT are given a sinusoidal voltage of  $V_{in} = 5\sin(2\pi ft) \text{ V}$  and the simulation is run for  $50 \text{ ns}$  with a time step of  $0.01 \text{ ns}$ . The output voltage  $V_{out}$  is taken from second and fourth electrode of the output IDT. The first and the third electrode of input and output IDT are grounded. To simulate mass loading a thin PMMA layer is placed over the mass loading region  $L_m$ . The height of PMMA layer is varied from  $200$  to  $250 \text{ nm}$  in steps of  $10 \text{ nm}$  and time response simulation is carried out for each of these heights. The time delay and the phase shift with respect to the plain surface is obtained and used to calculate the phase mass sensitivity of the device which is given by the relation [11]

$$S_{m\phi} = \lim_{\Delta m \rightarrow 0} \frac{1}{kD} \frac{\Delta\phi}{\Delta m} \quad (3)$$

where  $\Delta\phi$  denotes the phase shift occurring as a result of application of incremental mass per unit area  $\Delta m$  over the mass loading region and  $k$  is the wavevector. The impulse response of the device is obtained by applying a unit impulse of  $1.5 \text{ ns}$  width at the input IDT. The insertion loss (IL) of the device is found by taking the Fourier transform of the impulse response. The IL is calculated by the relation [12]

$$IL(dB) = 20 \log(|V_{out} / V_{in}|) \quad (4)$$

*Extra fine* tetrahedral elements are used for meshing the geometry which consists of about 26,000 elements with 210,000 degrees of freedom.

The properties of materials used in simulation are listed in Table 1.

**Table 1:** Properties of materials used in COMSOL simulation [13], [14]

Material	Density (kg/m <sup>3</sup> )	Young's modulus (GPa)	Poisson's ratio
SiO <sub>2</sub>	2200	60.84	0.17
PMMA	1180	3.3	0.35
<b><u>LiTaO<sub>3</sub> crystal properties</u></b>			
Elastic constants ( $\times 10^{10}$ N/m <sup>2</sup> )			
$\begin{bmatrix} 23.28 & 4.65 & 8.36 & -1.05 & 0 & 0 \\ 4.65 & 23.28 & 8.36 & 1.05 & 0 & 0 \\ 8.36 & 8.36 & 27.59 & 0 & 0 & 0 \\ -1.05 & 1.05 & 0 & 9.49 & 0 & 0 \\ 0 & 0 & 0 & 0 & 9.49 & -1.05 \\ 0 & 0 & 0 & 0 & -1.05 & 9.32 \end{bmatrix}$			
Piezoelectric constants (C/m <sup>2</sup> )			
$\begin{bmatrix} 0 & 0 & 0 & 0 & 2.64 & -1.86 \\ -1.86 & 1.86 & 0 & 2.64 & 0 & 0 \\ -0.22 & -0.22 & 1.71 & 0 & 0 & 0 \end{bmatrix}$			
Dielectric constants (in $\epsilon_0$ )			
$\begin{bmatrix} 40.9 & 0 & 0 \\ 0 & 40.9 & 0 \\ 0 & 0 & 42.5 \end{bmatrix}$			
Density = 7454 kg/m <sup>3</sup>			

## 4. Results and Discussion

The wave travels from input IDT to output IDT and the time snapshots at  $t = 4, 8, 12$  and  $16$  ns are shown in Fig. 3(a-d). The wave travels a distance of  $60 \mu\text{m}$  in about  $16$  ns giving a phase velocity of  $3750$  m/s. As the wave reaches the output IDT, it is critically damped in the adjacent layer so that there are no reflections from the edges of the device. The shear-horizontal nature of the Love wave is evident from the time response of the delay line. The input and output voltages are plotted in Fig. 4(a). The output voltage stabilizes after  $30$  ns. Application of  $5V$  sinusoidal input gives a stable  $0.82V$  sinusoidal output at the receiving IDT.

The normalized displacements at the output IDT are plotted in Fig. 4(b). It can be seen that the wave is shear-horizontal in nature since displacements in  $z$  direction are much greater than the vertical displacements in  $y$  direction.

The insertion loss of the delay line is calculated by applying a unit impulse at the input IDT and the obtained impulse response of the device is shown in Fig. 5(a). Next, the Fourier transform of the impulse response is performed to obtain the IL. The device exhibits an IL value of  $-32.2$  dB at  $326.9$  MHz as shown in Fig 5(b). As we move away from this frequency, the losses increased considerably.

To calculate the mass sensitivity of the device, a  $200$  nm thick PMMA layer was put over the delay area to simulate mass loading. The variation of output voltage with and without mass loading is shown in Fig. 6. It can be seen that the presence of PMMA layer causes a time delay of  $0.021$  ns with respect to the plain surface. The PMMA layer height is increased from  $200$  nm to  $250$  nm in steps of  $10$  nm. The corresponding values of time delay and phase shift are recorded and results are listed in Table 2. As per Eq. (3), the plot of  $\Delta\phi/kD$  versus  $\Delta m$  gives a straight line with the slope representing the phase mass sensitivity  $S_{m\phi}$ .

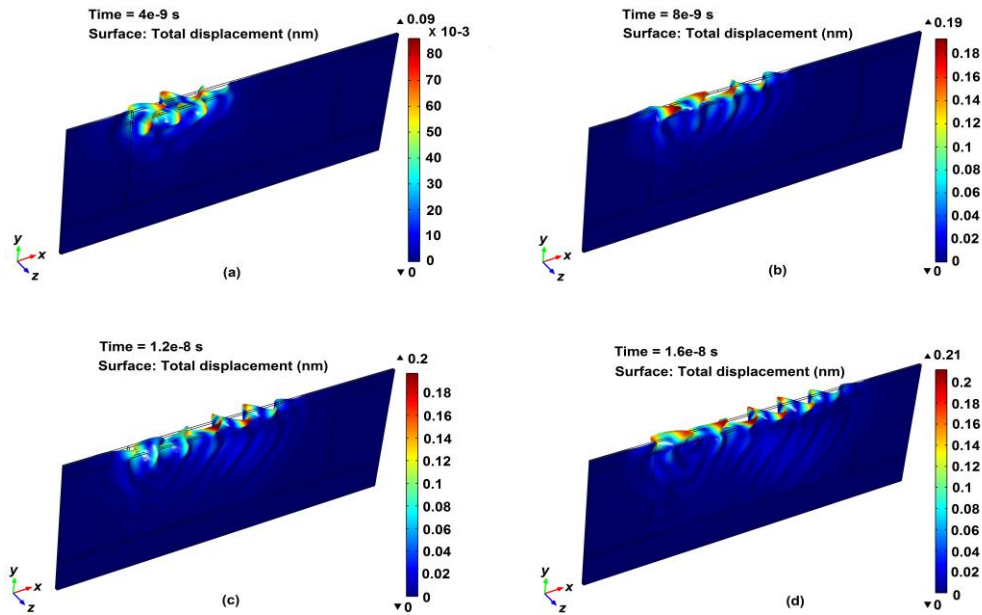


**Figure 3.** Snapshots of time response of Love wave delay line at (a) 4 ns (b) 8 ns (c) 12 ns and (d) 16 ns.

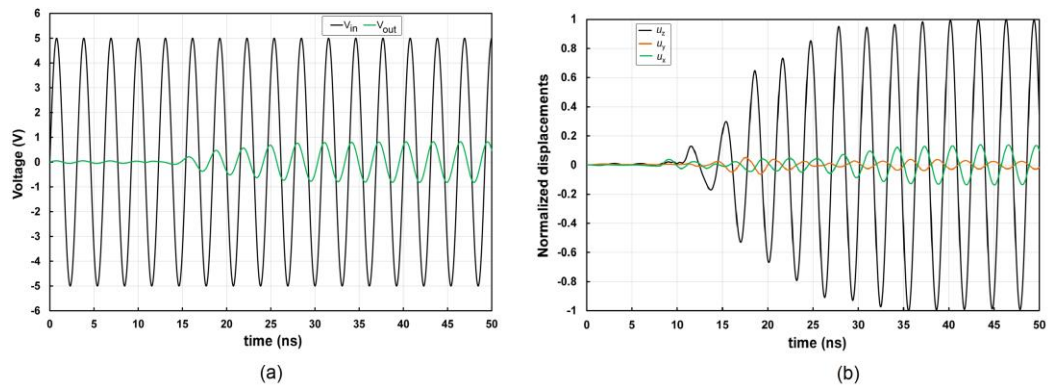


**Figure 4.** (a) Variation of input and output voltage with time. (b) Plot of normalized displacements  $u_x$ ,  $u_y$  and  $u_z$  at the output IDT with time.

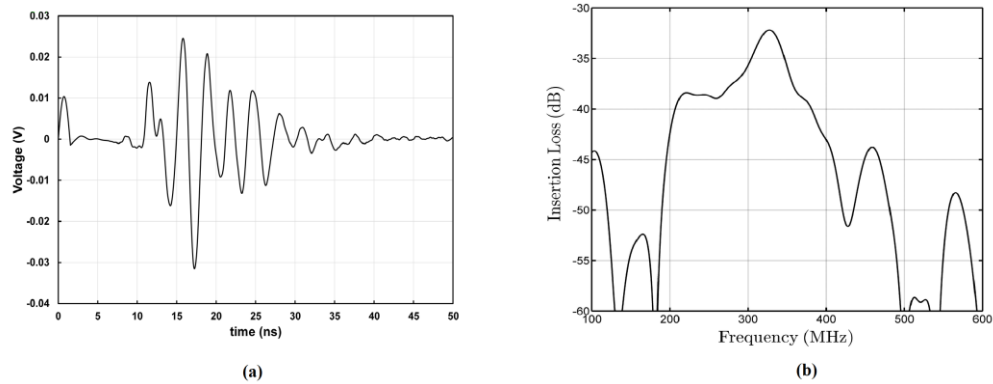


**Figure 5.** (a) Impulse response of the delay line (b) Insertion loss of the delay line.

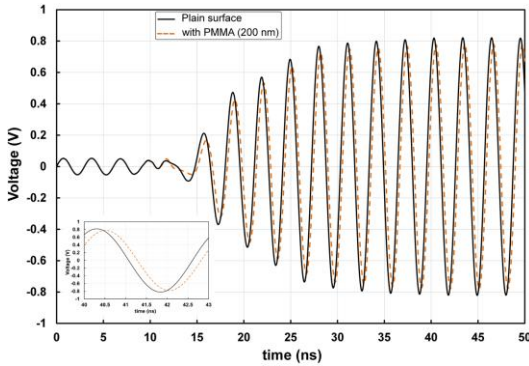


**Figure 6.** Plot of output voltage versus time for the plain surface and 200 nm thick PMMA loaded surface. Inset shows the time delay between two waveforms.

**Table 2:** Time delay and phase shift obtained upon loading the SAW Delay line with PMMA layer of different heights.

PMMA Height (nm)	Incremental mass per unit area $\Delta m$ (kg/m <sup>2</sup> )	Time delay $\Delta t$ (ns)	Phase shift $\Delta\phi$ (rad)
200	2.36E-04	0.2099	0.428623
210	2.48E-04	0.2196	0.448431
220	2.60E-04	0.2295	0.468647
230	2.71E-04	0.2384	0.486821
240	2.83E-04	0.2496	0.509692
250	2.95E-04	0.2586	0.52807

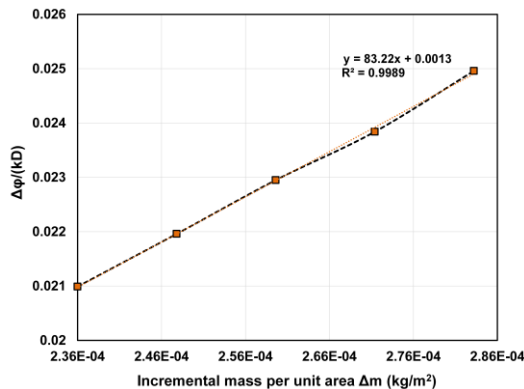


**Figure 7.** Plot of normalized phase shift ( $\Delta\phi/kD$ ) versus incremental mass per unit area ( $\Delta m$ ). The slope of the straight line represents the phase mass sensitivity.

This is shown in Fig. 7. The calculated value of  $S_{m\phi}$  is 83.22 m<sup>2</sup>/kg. The phase mass sensitivity

can be converted into the frequency mass sensitivity  $S_m$  by using the relation [11]

$$S_m = \left( \frac{D}{L} \right) S_{m\phi} \quad (5)$$

This gives a frequency mass sensitivity of 54.09 m<sup>2</sup>/kg which is consistent with values typically reported for Love wave devices [13], [15], [16].

## 5. Conclusions

The paper has presented finite element simulation of Love wave based SAW Delay device comprising of 36°-YX LT substrate with 4.7  $\mu\text{m}$  thick SiO<sub>2</sub> guiding layer. Typically delay line simulation requires large geometry and memory usage but using periodic boundary conditions in COMSOL aids to keep the geometry small. We perform the time response study to calculate the normalized displacement and output voltage that confirms the shear-horizontal nature of Love wave. The device gives a phase velocity of 3750 m/s, phase mass sensitivity of 83.22 m<sup>2</sup>/kg and IL of -32.2 dB. Love wave devices are very important for designing biosensors and simulation of SAW devices using COMSOL can help to obtain the device characteristics prior to actual fabrication.

## 6. Acknowledgement

The authors would like to thank Department of Electronics and Information Technology (No. 5(9)/2012-NANO (Vol. II), Government of India for financial support.

## 7. References

- [1] R. M. White and F. W. Voltmer, "Direct Piezoelectric Coupling To Surface Elastic Waves," *Appl. Phys. Lett.*, vol. 7, no. 12, p. 314, 1965.
- [2] K. Lange, B. E. Rapp, and M. Rapp, "Surface acoustic wave biosensors: a review.," *Anal. Bioanal. Chem.*, vol. 391, no. 5, pp. 1509–19, Jul. 2008.

- [3] C. Campbell, *Surface acoustic wave devices and their signal processing applications*. Academic press, 1989.
- [4] D. Morgan, *Surface acoustic wave filters*. 2010.
- [5] B. Jakoby and M. J. Vellekoop, "Properties of Love waves: applications in sensors," *Smart Mater. Struct.*, vol. 6, no. 6, pp. 668–679, Dec. 1997.
- [6] K. Länge, B. E. Rapp, and M. Rapp, "Surface acoustic wave biosensors: A review," *Anal. Bioanal. Chem.*, vol. 391, no. 5, pp. 1509–1519, 2008.
- [7] G. McHale, M. I. Newton, F. Martin, E. Gizeli, and K. a. Melzak, "Resonant conditions for Love wave guiding layer thickness," *Appl. Phys. Lett.*, vol. 79, no. 21, p. 3542, 2001.
- [8] G. L. Harding, J. Du, P. R. Dencher, D. Barnett, and E. Howe, "Love wave acoustic immunosensor operating in liquid," *Sensors Actuators A Phys.*, vol. 61, no. 1–3, pp. 279–286, Jun. 1997.
- [9] M. Hofer, N. Finger, G. Kovacs, J. Schöberl, S. Zaglmayr, U. Langer, and R. Lerch, "Finite-element simulation of wave propagation in periodic piezoelectric SAW structures," *IEEE Trans. Ultrason. Ferroelectr. Freq. Control*, vol. 53, no. 6, pp. 1192–1200, 2006.
- [10] www.comsol.com, "COMSOL Multiphysics v4.4." .
- [11] M.-I. Rocha-Gaso, R. Fernandez-Diaz, a. Arnau-Vives, and C. March-Iborra, "Mass sensitivity evaluation of a Love wave sensor using the 3D Finite Element Method," *2010 IEEE Int. Freq. Control Symp.*, pp. 228–231, Jun. 2010.
- [12] I.-Y. Huang, C.-Y. Lin, and J.-W. Lan, "Improving thin-film zinc-oxide surface acoustic wave device insertion loss using a grooved reflective grating structure," *J. Micro/Nanolithography, MEMS, MOEMS*, vol. 12, no. 1, p. 013019, Mar. 2013.
- [13] M. Gaso, Y. Jiménez, L. Francis, and A. Arnau, "Love Wave Biosensors: A Review," 2013.
- [14] G. Kovacs, M. Anhorn, H. E. Engan, G. Visintini, and C. C. W. Ruppel, "Improved material constants for LiNbO<sub>3</sub> and LiTaO<sub>3</sub>," *IEEE Symp. Ultrason.*, pp. 435–438, 1990.
- [15] J. W. Grate, S. J. Martin, and R. M. White, "Acoustic Wave Microsensors Part II," *Anal. Chem.*, vol. 65, no. 22, p. 987A–996A, 1993.
- [16] N. Barié, T. Wessa, M. Bruns, and M. Rapp, "Love waves in SiO<sub>2</sub> layers on STW-resonators based on LiTaO<sub>3</sub>," *Talanta*, vol. 62, no. 1, pp. 71–79, Jan. 2004.